


Toolbox for elementary fermions with a dipolar Fermi gas in a three-dimensional optical latticeShuai Li, Maksims Arzamasovs, Hongrong Li, Fuli Li, and Bo Liu ^{*}*MOE Key Laboratory for Nonequilibrium Synthesis and Modulation of Condensed Matter
and Shaanxi Province Key Laboratory of Quantum Information and Quantum Optoelectronic Devices,
School of Physics, Xi'an Jiaotong University, Xi'an 710049, China* (Received 18 May 2021; revised 3 August 2021; accepted 5 August 2021; published 10 September 2021)

There has been growing interest in investigating properties of elementary particles predicted by the standard model. Examples of such studies include exploring their low-energy analogs in a condensed-matter system, where they arise as collective states or quasiparticles. Here we show that a toolbox for systematically engineering the emergent elementary fermions, i.e., Dirac, Weyl, and Majorana fermions, can be built in a single atomic system composed of a spinless magnetic dipolar Fermi gas in a three-dimensional optical lattice. The designed direction-dependent dipole-dipole interaction leads to both the basic building block, i.e., in-plane $p + ip$ superfluid pairing instability, and the manipulating tool, i.e., out-of-plane Peierls instability. It is shown that the Peierls instability provides a natural way of tuning the topological nature of $p + ip$ superfluids and can transform the fermion's nature between distinct emergent particles. Our scheme should contribute to the search for elementary particles through manipulating the topology.

DOI: [10.1103/PhysRevA.104.033312](https://doi.org/10.1103/PhysRevA.104.033312)**I. INTRODUCTION**

Fundamental particles are either the building blocks of matter, called fermions, or the mediators of interactions, called bosons. These elementary particles, such as Dirac, Weyl, and Majorana fermions [1–5], can be understood within the framework of the relativistic quantum field theory [6,7]. However, only Dirac fermions have been observed as elementary particles in nature so far. For many years now, another promising approach to observe particle properties that have no realization in elementary particles is the investigation of their low-energy analogous quasiparticles, such as in condensed matter or atomic systems. It paves a different way for exploring fundamental particles without paying the steep price of a high-energy particle collider and thus has attracted a tremendous amount of research interest in various fields of physics. There has been some exciting progress in the search for the emergent Dirac, Weyl, and Majorana fermions. Recent examples include graphene [8–13], several topological phases in solids containing quantum Hall states, topological insulators and superconductors, etc. [14–16]. Another exciting perspective is the recent realization of artificial materials such as cold atoms [17–35] or photonic crystals [36,37]. However, finding a single material that can systematically transform the fermion's nature and realize distinct elementary fermions in its equilibrium state is highly nontrivial and still stands as an obstacle yet to be overcome.

Here we show that ultracold gases of magnetic dipolar atoms or polar molecules, as presently developed in the laboratory, provide us with opportunities for constructing a toolbox for systematically engineering all three kinds of el-

ementary fermions listed above. The attractiveness of this idea rests on the fact that the strength and even the sign of dipolar interaction in cold atoms are highly tunable [38]. The direction of dipole moments can be fixed by applying an external magnetic field. Let the external field be orientated at a small angle with respect to the xy plane and rotate fast around the z axis. The time-averaged interaction between dipoles is isotropically attractive in the xy plane and repulsive in the z direction. Such a scheme has been realized in the experimental system of dysprosium atoms [39]. In general, the xy -plane attraction is expected to cause superfluid pairing instability and leads to an in-plane $p + ip$ superfluid in a spinless dipolar Fermi gas. The repulsion should restrict the pairing in the z direction and results in the Peierls instability in the presence of lattice potential. Such a spontaneously formed density modulation provides a natural tool to manipulate the topological nature of $p + ip$ superfluids and thus allows us to build a toolbox for systematically engineering all three of the above kinds of elementary fermions through tuning the topology of our proposed single atomic system. Such a heuristically argued result is indeed confirmed by our detailed analysis through the model to be introduced below.

II. EFFECTIVE MODEL

Consider a spinless dipolar Fermi gas, such as ^{161}Dy [40,41] or ^{167}Er [42,43], subjected to an external rotating magnetic field $\mathbf{B}(t) = B[\hat{z} \cos \varphi + \sin \varphi(\hat{x} \cos \Omega t + \hat{y} \sin \Omega t)]$, where Ω is the rotation frequency, B is the magnitude of the magnetic field, z is the rotation axis, and φ is the angle between the magnetic field and the z axis. In strong magnetic fields, dipoles are aligned parallel to $\mathbf{B}(t)$. With fast rotations, i.e., Ω being much larger than typical frequencies of particle motion and simultaneously much

^{*}liubophy@gmail.com

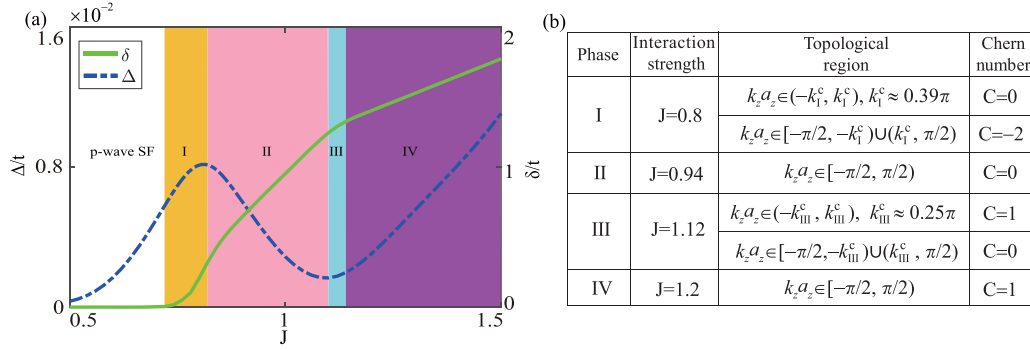


FIG. 1. (a) Zero-temperature phase diagram as a function of dipolar interaction strength at average filling $n_0 = 0.6$. The dashed and solid lines stand for the pairing and CDW order parameters, respectively. The spontaneously formed density modulation serves as a natural tool to manipulate the topological nature of the system, leading to distinct topological phases marked by various colors. (b) Table of examples showing the distinct topological nature of various phases in (a). The other parameters are $t_z/t = 0.5$ and $a_z/a = 3.5$.

smaller than the level splitting in the field, the effective interaction between dipoles is the time-averaged interaction $V(\mathbf{r}) = \frac{d^2(3\cos^2\varphi-1)}{2r^3}(1-3\cos^2\theta) \equiv \frac{d^2}{r^3}(1-3\cos^2\theta)$, where $d^2 \equiv d^2 \frac{3\cos^2\varphi-1}{2}$, with the magnetic dipole moment d . Here \mathbf{r} is the vector connecting two dipolar particles and θ is the angle between \mathbf{r} and the z axis. The effective in-plane attraction is created by making $\cos\varphi < \sqrt{1/3}$, which can be realized by changing the amplitudes of static and rotating parts of the magnetic field. We further consider these dipolar atoms loaded in a three-dimensional optical lattice $V_{\text{opt}}(\mathbf{r}) = -V_0[\cos^2(k_{Lx}x) + \cos^2(k_{Ly}y)] - V_{0z}\cos^2(k_{Lz}z)$, where k_{Lx} , k_{Ly} , and k_{Lz} are wave vectors of laser fields and the corresponding lattice constants are defined as $a_x = \pi/k_{Lx}$, $a_y = \pi/k_{Ly}$, and $a_z = \pi/k_{Lz}$. Here V_0 and V_{0z} are lattice depths in the xy plane and z direction, respectively. In this work, we consider an anisotropic three-dimensional (3D) lattice with $a_x = a_y \equiv a < a_z$. When the lattice depths are large enough, the system can be described by the Fermi-Hubbard model in the tight-binding regime

$$\mathbf{H} = - \sum_{\alpha=x,y,z} \sum_i t_\alpha (c_i^\dagger c_{i+e_\alpha} + \text{H.c.}) - \mu \sum_i c_i^\dagger c_i + \frac{1}{2} \sum_{i \neq j} V_{i-j} c_i^\dagger c_j^\dagger c_j c_i, \quad (1)$$

where $t_x = t_y \equiv t$ and t_z are the hopping amplitudes describing tunneling in the x , y , and z directions, respectively; $i \equiv (i_x, i_y, i_z)$ is the site index denoting the lattice site $\mathbf{R}_i \equiv (a_i x, a_i y, a_i z)$; μ is the chemical potential; and e_α represents the unit vector. The dipole-dipole interaction is given by $V_{i-j} = d^2 \frac{|\mathbf{R}_i - \mathbf{R}_j|^2 - 3(i_z - j_z)^2 a_z^2}{|\mathbf{R}_i - \mathbf{R}_j|^5}$.

A. Self-consistent Hartree-Fock-Bogoliubov method

To study the many-body instabilities of the Hamiltonian (1), we perform both mean-field theory and Monte Carlo (MC) simulations. By employing the self-consistent Hartree-Fock-Bogoliubov (HFB) method, the zero-temperature phase diagram is obtained as shown in Fig. 1(a). Furthermore, distinct many-body phases in Fig. 1(a) are identified through MC simulations. In the HFB method, the Peierls instability can be described by writing the density distribution of the system as

$n_i = n_0 + C \cos(\mathbf{Q} \cdot \mathbf{R}_i)$, where \mathbf{Q} represents the periodicity of density pattern and $n_0 = \sum_i \langle c_i^\dagger c_i \rangle / N_L$ is the average filling, with N_L denoting total lattice site. The order parameter describing this charge density wave (CDW) can thus be defined as $\delta_{\pm\mathbf{Q}} = V(\pm\mathbf{Q})C/2$, where $V(\mathbf{k}) = \sum_{n \neq 0} V_n \exp(-i\mathbf{k} \cdot \mathbf{r}_n)$. We also introduce the superfluid pairing order parameter as $\Delta(\mathbf{k}) = \frac{1}{N_L} \sum_{\mathbf{k}'} V(\mathbf{k} - \mathbf{k}') \langle c_{-\mathbf{k}} c_{\mathbf{k}'} \rangle$, where $\langle \dots \rangle$ means the expectation value in the ground state. Then the Hamiltonian (1) can be further expressed in the mean-field approximation as

$$\mathbf{H}_{\text{MF}} = \sum_{\mathbf{k}} \xi_{\mathbf{k}} c_{\mathbf{k}}^\dagger c_{\mathbf{k}} + \sum_{\mathbf{k}} \left(\frac{\Delta(\mathbf{k})}{2} c_{\mathbf{k}}^\dagger c_{-\mathbf{k}}^\dagger + \text{H.c.} \right) + \sum_{\mathbf{Q}_m = \pm\mathbf{Q}} \sum_{\mathbf{k}} \left(\frac{\delta_{\mathbf{Q}_m}}{2} c_{\mathbf{k}}^\dagger c_{\mathbf{k}+\mathbf{Q}_m} + \text{H.c.} \right) - E_I, \quad (2)$$

where $\xi_{\mathbf{k}} = \varepsilon_{\mathbf{k}} + \Sigma_{\mathbf{k}} - \mu$, with the band energy $\varepsilon_{\mathbf{k}} = -2t(\cos k_x a + \cos k_y a) - 2t_z \cos k_z a$, μ the chemical potential, and $\Sigma_{\mathbf{k}}$ the Hartree-Fock self-energy given by $\Sigma_{\mathbf{k}} = V(0)n_0 - \frac{1}{N_L} \sum_{\mathbf{k}'} V(\mathbf{k} - \mathbf{k}') n_{\mathbf{k}'}$, with $V(0) = \sum_{n \neq 0} V_n$. For example, $V(0) = -5.62Jt$ when $a_z/a = 3.5$, where $J \equiv |d^2/(ta^3)|$ captures the strength of the dipolar interaction. In addition, $E_I = \frac{1}{2} \sum_{i \neq j} V_{i-j} (n_i n_j - |\langle c_i^\dagger c_j \rangle|^2 + |\langle c_j c_i \rangle|^2)$. The mean-field Hamiltonian (2) can be diagonalized through the Bogoliubov transformation and the corresponding eigenenergies are labeled as E_n . Straightforward calculations lead to the mean-field thermodynamic potential $\Omega_{\text{MF}} = -\frac{k_B T}{4} \sum_n \ln[1 + \exp(-\frac{E_n}{k_B T})] + \frac{1}{2} \sum_{\mathbf{k}} \xi_{\mathbf{k}} - E_I$. In the $T \rightarrow 0$ limit, $-k_B T \sum_n \ln[1 + \exp(-\frac{E_n}{k_B T})] = \sum_n E_n \Theta(-E_n)$, with the Heaviside step function Θ .

The order parameters defined above can be obtained by minimizing Ω_{MF} and the average filling of the system can be determined by the relation $n_0 = -\frac{1}{N_L} \frac{\partial \Omega_{\text{MF}}}{\partial \mu}$. We find that the period of the CDW order is highly tunable through simply changing the average filling of the system. There is a region of n_0 , i.e., $0.5 \leq n_0 < n_A \approx 0.67$, where \mathbf{Q} is located at $\mathbf{Q} = (0, 0, \pi/a_z)$. For example, as shown in Fig. 2(a), when $n_0 = 0.6$, the mean-field thermodynamic potential is minimized at $\mathbf{Q} = (0, 0, \pi/a_z)$, indicating that the density modulation is in the z direction and its period is $2a_z$. When further increasing n_0 , i.e., $n_A < n_0 < n_B \approx 0.85$, the period of the z -directional CDW order can be changed to $3a_z$. For instance, as shown in

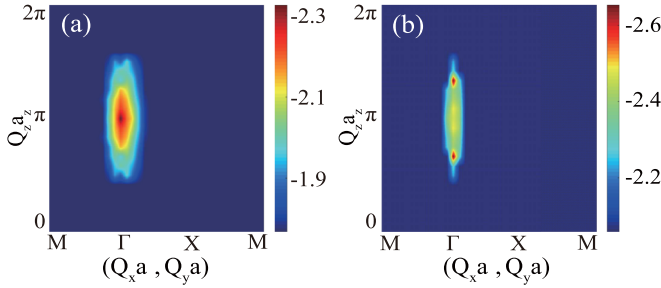


FIG. 2. Mean-field energy of the model Hamiltonian in Eq. (2) as a function of \mathbf{Q} for (a) $n_0 = 0.6$ and $J = 1.1$ and (b) $n_0 = 0.73$ and $J = 1.1$. The other parameters are the same as in Fig. 1.

Fig. 2(b), when $n_0 = 0.73$, the mean-field thermodynamic potential is minimized at $\mathbf{Q} = (0, 0, 2\pi/3a_z)$. We also find that the superfluid order parameter $\Delta(\mathbf{k})$ behaves like an in-plane $p + ip$ superfluid, i.e., $\Delta(\mathbf{k}) = \Delta(k_z)[\sin(k_x a) + i \sin(k_y a)]$, where $\Delta(k_z)$ records very slight variation for different k_z as shown in Fig. 3. Therefore, we can express the superfluid order parameter as $\Delta[\sin(k_x a) + i \sin(k_y a)]$. Note that in the HFB method the momentum grid is chosen as $120 \times 120 \times 120$ to perform the lattice momentum summation, which is a sufficiently large size, since both pairing and CDW orders have already converged, as shown in Fig. 4.

B. Variational Monte Carlo method

To further verify the existence of CDW and superfluid orders, we have performed a variational Monte Carlo (VMC) [44–48] calculation on an $8 \times 8 \times 8$ lattice system with periodic boundary conditions. The VMC method is one of the promising methods to study strongly correlated systems and there is no sign problem in studies of fermionic systems since the weight of Monte Carlo sampling is positive definite. To simplify the simulation, we consider the strongest dipole-dipole interaction between nearest neighbors.

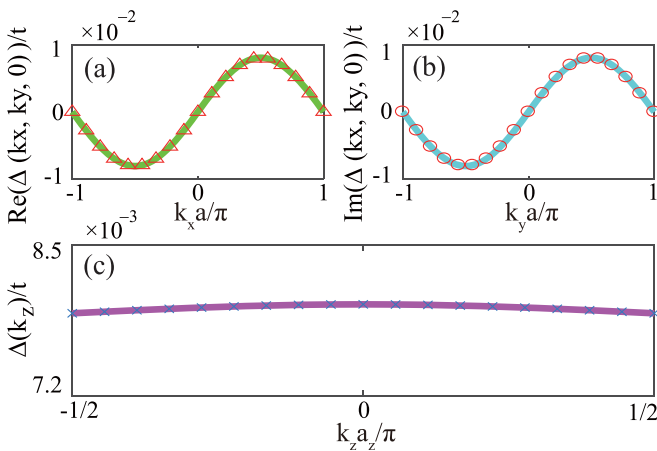


FIG. 3. Pairing order parameter $\Delta(\mathbf{k})$ as a function of momentum. (a) and (b) Plot of $\Delta(\mathbf{k})$ behaving like an in-plane $p + ip$ superfluid; here we choose $k_z a_z = 0$. (c) Slight variation of the pairing order parameter along the k_z axis, where $k_x a = \pi/2$ and $k_y a = 0$. The other parameters are $J = 0.78$, $n_0 = 0.6$, $t_z/t = 0.5$, and $a_z/a = 3.5$.

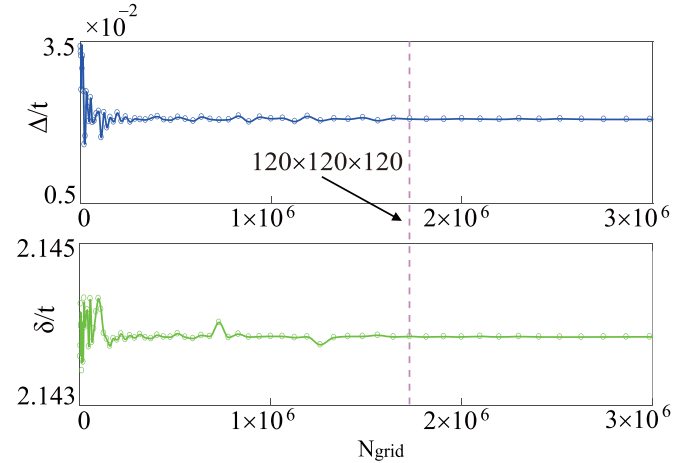


FIG. 4. Momentum grid N_{grid} chosen as $120 \times 120 \times 120$ to perform the lattice momentum summation in the HFB calculation. It is sufficiently large where both pairing and CDW orders have already converged. Here $J = 1.8$ and the other parameters are the same as in Fig. 1.

The wave function employed in our many-variable variational Monte Carlo simulation [44,45] can be expressed as $|\phi_{\text{ref}}\rangle = \mathcal{P}_J |\phi_{\text{pair}}\rangle$, where $|\phi_{\text{pair}}\rangle = (\sum_{i,j=1}^{N_L} f_{ij} c_i^\dagger c_j^\dagger)^{N/2} |0\rangle$ is the Pfaffian pairing wave function [46] and $\mathcal{P}_J = \exp[\frac{1}{2} \sum_{i \neq j} v_{ij} (n_i - 1)(n_j - 1)]$ is the Jastrow factor [47], which accounts for long-range density correlations. Here N refers to the number of fermions. Such a flexible variational wave function with a large number of variational parameters can be simultaneously optimized by using the stochastic reconfiguration method [48], which can be applied to efficiently compute the ground state of our proposed system.

To investigate the superfluid pairing order in the ground state, we study the pairing correlation defined as

$$P(\mathbf{R}_{\parallel}) = \frac{1}{2N_L} \sum_{\mathbf{R}_i} \langle \Delta^\dagger(\mathbf{R}_i) \Delta(\mathbf{R}_i + \mathbf{R}_{\parallel}) + \Delta(\mathbf{R}_i) \Delta^\dagger(\mathbf{R}_i + \mathbf{R}_{\parallel}) \rangle,$$

with $\Delta(\mathbf{R}_i) \equiv c_i c_{i+e_x} - c_i c_{i-e_x} + i(c_i c_{i+e_y} - c_i c_{i-e_y})$ capturing the in-plane $p + ip$ symmetry of the superfluid pairing. Here \mathbf{R}_{\parallel} is an in-plane vector. As shown in Fig. 5(a), the

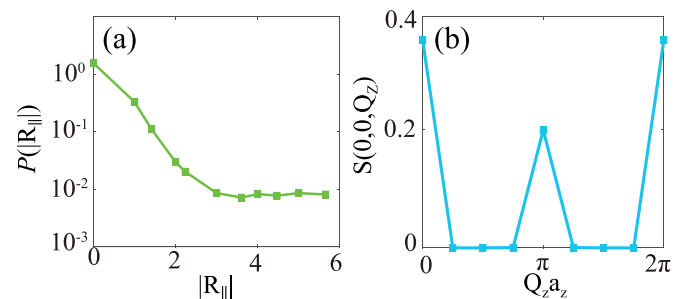


FIG. 5. (a) In-plane superconducting correlation $P(|\mathbf{R}_{\parallel}|)$ as a function of $|\mathbf{R}_{\parallel}|$. Here $P(|\mathbf{R}_{\parallel}|)$ shows saturated long-range correlation, indicating the existence of in-plane $p + ip$ superfluid pairing order. (b) Structure factor $S(\mathbf{Q})$ as a function of momentum, where its peak is located at $(0, 0, \pi/a_z)$, indicating the existence of the z -directional CDW order with the period being $2a_z$. Here $J = 1.2$ and the other parameters are the same as in Fig. 1.

long-range saturation behavior of the in-plane pairing correlation $P(\mathbf{R}_{\parallel})$ indicates the existence of superfluid pairing order in the ground state. To identify the existence of CDW order in the ground state, we calculate the density structure factor defined as

$$S(\mathbf{Q}) = \frac{1}{N_L^2} \sum_{i,j} \langle c_i^\dagger c_i c_j^\dagger c_j \rangle e^{i\mathbf{Q} \cdot (\mathbf{R}_i - \mathbf{R}_j)}.$$

The peak in density structure factor provides information on the CDW order. As shown in Fig. 5(b), the structure factor $S(\mathbf{Q})$ is peaked at $(0, 0, \pi/a_z)$, indicating the existence of a z -directional density modulation pattern with the period of $2a_z$, which is consistent with our mean-field calculation as shown in Fig. 1(a).

III. PHYSICAL MECHANISM FOR TUNING THE TOPOLOGICAL NATURE

To understand how we can utilize the spontaneously formed density modulation as a tool to manipulate the topological nature of the system, let us start with our basic building block, i.e., in-plane $p + ip$ superfluids. It is known that the topology of 2D $p + ip$ superfluids can be changed by tuning the system filling and thus results in distinct topological regions: a topological trivial region and two distinct topological regions with opposite chirality [49]. In our proposed system, the spontaneously formed z -directional density modulation can serve as a natural tool to tune the fillings of $p + ip$ superfluid layers through effectively altering their respective chemical potential and thus changes their topological nature, which is confirmed by our detailed analysis below.

For instance, let us consider the case of the period of z -directional density modulation being $2a_z$, i.e., $\mathbf{Q} = (0, 0, \pi/a_z)$. The topology of the system can be understood through the Bogoliubov–de Gennes (BdG) Hamiltonian, which can be expressed as

$$H_{\text{BdG}}^\pi = \begin{pmatrix} \xi_{\mathbf{k}} & \Delta(\mathbf{k}) & 2\delta & 0 \\ \Delta^*(\mathbf{k}) & -\xi_{-\mathbf{k}} & 0 & -2\delta \\ 2\delta & 0 & \xi_{\mathbf{k}+\mathbf{Q}} & \Delta(\mathbf{k}) \\ 0 & -2\delta & \Delta^*(\mathbf{k}) & -\xi_{-\mathbf{k}-\mathbf{Q}} \end{pmatrix}, \quad (3)$$

where the Nambu spinors are chosen as $(c_{\mathbf{k}}^\dagger, c_{-\mathbf{k}}, c_{\mathbf{k}+\mathbf{Q}}^\dagger, c_{-\mathbf{k}-\mathbf{Q}})$. A unitary transformation can be applied to the BdG Hamiltonian above and we obtain

$$\tilde{H}_{\text{BdG}}^\pi = T_\pi^\dagger H_{\text{BdG}}^\pi T_\pi = \begin{pmatrix} \xi_{\mathbf{k}} & 2\delta & \Delta(\mathbf{k}) & 0 \\ 2\delta & \xi_{\mathbf{k}+\mathbf{Q}} & 0 & \Delta(\mathbf{k}) \\ \Delta^*(\mathbf{k}) & 0 & -\xi_{-\mathbf{k}} & -2\delta \\ 0 & \Delta^*(\mathbf{k}) & -2\delta & -\xi_{-\mathbf{k}-\mathbf{Q}} \end{pmatrix},$$

with

$$T_\pi = \begin{pmatrix} 1 & 0 & 0 & 0 \\ 0 & 0 & 1 & 0 \\ 0 & 1 & 0 & 0 \\ 0 & 0 & 0 & 1 \end{pmatrix}.$$

Then $\tilde{H}_{\text{BdG}}^\pi$ can be rewritten as

$$\tilde{H}_{\text{BdG}}^\pi = \begin{pmatrix} H_{\text{CDW}}^\pi & \Delta_k^{2 \times 2} \\ \Delta_k^{*2 \times 2} & -H_{\text{CDW}}^\pi \end{pmatrix},$$

where $H_{\text{CDW}}^\pi = \begin{pmatrix} \xi_{\mathbf{k}} & 2\delta \\ 2\delta & \xi_{\mathbf{k}+\mathbf{Q}} \end{pmatrix}$ and $\Delta_k^{2 \times 2} = \Delta(\mathbf{k}) I_{2 \times 2}$, with $I_{2 \times 2}$ the 2×2 unit matrix. We then apply another unitary transformation to $\tilde{H}_{\text{BdG}}^\pi$ and obtain that

$$\mathcal{H}_{\text{BdG}}^{\prime\pi} = \Gamma_\pi^\dagger \tilde{H}_{\text{BdG}}^\pi \Gamma_\pi = \begin{pmatrix} E_1^\pi & 0 & \Delta(\mathbf{k}) & 0 \\ 0 & E_2^\pi & 0 & \Delta(\mathbf{k}) \\ \Delta^*(\mathbf{k}) & 0 & -E_1^\pi & 0 \\ 0 & \Delta^*(\mathbf{k}) & 0 & -E_2^\pi \end{pmatrix},$$

where the unitary transformation is defined as $\Gamma_\pi = \begin{pmatrix} \Gamma_{\pi\text{CDW}} & 0_{2 \times 2} \\ 0_{2 \times 2} & \Gamma_{\pi\text{CDW}} \end{pmatrix}$. Further, $\Gamma_{\pi\text{CDW}}$ can be constructed from the relation $\Gamma_{\pi\text{CDW}}^\dagger H_{\text{CDW}}^\pi \Gamma_{\pi\text{CDW}} = \begin{pmatrix} E_1^\pi(\mathbf{k}) & 0 \\ 0 & E_2^\pi(\mathbf{k}) \end{pmatrix}$, with $E_1^\pi(\mathbf{k}) = \frac{\xi_{\mathbf{k}} + \xi_{\mathbf{k}+\mathbf{Q}}}{2} - \sqrt{4\delta^2 + \left(\frac{\xi_{\mathbf{k}} - \xi_{\mathbf{k}+\mathbf{Q}}}{2}\right)^2}$ and $E_2^\pi(\mathbf{k}) = \frac{\xi_{\mathbf{k}} + \xi_{\mathbf{k}+\mathbf{Q}}}{2} + \sqrt{4\delta^2 + \left(\frac{\xi_{\mathbf{k}} - \xi_{\mathbf{k}+\mathbf{Q}}}{2}\right)^2}$. After applying the unitary transformation T_π to $\mathcal{H}_{\text{BdG}}^{\prime\pi}$, we eventually obtain

$$\begin{aligned} \mathcal{H}_{\text{BdG}}^\pi &= T_\pi^\dagger \mathcal{H}_{\text{BdG}}^{\prime\pi} T_\pi = \begin{pmatrix} E_1^\pi & \Delta(\mathbf{k}) & 0 & 0 \\ \Delta^*(\mathbf{k}) & -E_1^\pi & 0 & 0 \\ 0 & 0 & E_2^\pi & \Delta(\mathbf{k}) \\ 0 & 0 & \Delta^*(\mathbf{k}) & -E_2^\pi \end{pmatrix} \\ &\equiv \begin{pmatrix} H_{p\text{-wave}}^{\prime\pi} & 0_{2 \times 2} \\ 0_{2 \times 2} & H_{p\text{-wave}}^{\prime\prime\pi} \end{pmatrix}. \end{aligned} \quad (4)$$

Here $\mathcal{H}_{\text{BdG}}^\pi$ clearly shows that the topology of the system can be engineered by simultaneously manipulating the two effective Hamiltonians $H_{p\text{-wave}}^{\prime\pi}$ and $H_{p\text{-wave}}^{\prime\prime\pi}$, describing in-plane $p + ip$ superfluids. This can be naturally achieved via the spontaneously formed density modulation in our proposed scheme. To show this, let us consider the Hamiltonian $\mathcal{H}_{\text{BdG}}^\pi$ at a fixed k_z . The topologically distinct regions of $p + ip$ superfluids Hamiltonian $H_{p\text{-wave}}^{\prime\pi}$ ($H_{p\text{-wave}}^{\prime\prime\pi}$) are (i) $\mu'(\mu'') < -4t'$ and $\mu'(\mu'') > 4t'$, which are the topological trivial region, and (ii) $-4t' < \mu'(\mu'') < 0$ and $0 < \mu'(\mu'') < 4t'$, which are the topological regions with opposite chirality. Here $\mu' = \tilde{\mu} - \sqrt{4\delta^2 + (-2t'_z \cos k_z a_z)^2}$ and $\mu'' = \tilde{\mu} + \sqrt{4\delta^2 + (-2t'_z \cos k_z a_z)^2}$ with the effective hoppings $t'_\alpha = t_\alpha - \Sigma_\alpha/2$, $t' \equiv t'_x = t'_y$, and $\tilde{\mu} = \mu - V(0)n_0$. Note that to simplify the discussion we consider the strongest exchange interaction energy between nearest neighbors as $\Sigma_{x(y)} = \sum_{\mathbf{k}} \frac{2J}{N_L} \cos(k_x(y)a) n_{\mathbf{k}}$ and $\Sigma_z = -\sum_{\mathbf{k}} \frac{4Ja_z^3}{N_L a_z^2} \cos(k_z a_z) n_{\mathbf{k}}$, with $J \equiv |d^2/ta^3|$ capturing the strength of dipolar interaction.

The two effective chemical potentials μ' and μ'' can be tuned simultaneously by changing the CDW order δ via varying J and thus can manipulate the topology of the system. For example, considering the case of $J = 0.8$ in Fig. 1(a), the CDW order δ simultaneously tunes the two effective chemical potentials in different regions: (i) $-\pi/2 \leq k_z a_z < -k_f^c \simeq 0.39\pi$ or $k_f^c < k_z a_z < \pi/2$, where $0 < \mu'(\mu'') < 4t'$, and $H_{p\text{-wave}}^{\prime\pi}$ and $H_{p\text{-wave}}^{\prime\prime\pi}$ are thus simultaneously engineered in the same topological region with Chern number $C = -1$, and (ii) $-k_f^c < k_z a_z < k_f^c$, where $-4t' < \mu' < 0$ and $0 < \mu'' < 4t'$, and $H_{p\text{-wave}}^{\prime\pi}$ and $H_{p\text{-wave}}^{\prime\prime\pi}$ are thus tuned in topological regions with opposite chirality characterized by $C = \pm 1$. Therefore, a topological phase [phase I in Fig. 1(a)] characterized by the existence of a topological phase transition between two topological regions with $C = -2$ and $C = 0$ along the k_z axis is achieved. While increasing J , for instance, to $J = 1.2$,

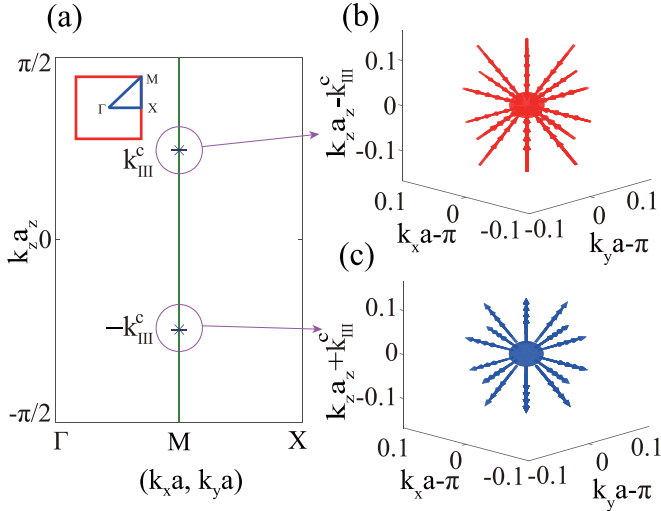


FIG. 6. (a) Gapless points of the quasiparticle excitation in phase III. The inset shows a contour in the (k_x, k_y) plane. (b) and (c) Hedgehoglike topological defects formed by the vector \mathbf{d} around two Weyl nodes. The interaction strength $J = 1.12$. The other parameters are the same as in Fig. 1.

the CDW order increases and plays a dominant role in tuning effective chemical potentials. Distinct from smaller J , here, for each k_z within the Brillouin zone, the effective chemical potentials are set in the same region as $-4t' < \mu' < 0$ and $\mu'' > 4t'$. Thus $H_{p\text{-wave}}^{\prime\prime\pi}$ and $H_{p\text{-wave}}^{\prime\prime\pi}$ are simultaneously engineered in a topological region with $C = 1$ and a non-topological region with $C = 0$, respectively. Therefore, a new topological phase [phase IV in Fig. 1(a)] characterized by a uniform Chern number ($C = 1$) is obtained. Using the same approach, two other topological phases [phases II and III in Fig. 1(a)] can be determined. We also find that there is a threshold of J , below which $\delta = 0$, where the p -wave superfluid is favored. We can map out the zero-temperature phase diagram as shown in Fig. 1(a). Such an analysis is readily generalizable to the case $\mathbf{Q} = (0, 0, 2\pi/3a_z)$. Another four distinct topological phases have been obtained (see details in Appendix A), indicating that our scheme provides a systematic way of engineering the topological nature of the system.

IV. TOOLBOX FOR ENGINEERING ELEMENTARY FERMIONS

A. Weyl fermions

We now show how to engineer three kinds of elementary fermions, i.e., Dirac, Weyl, and Majorana fermions, through manipulating the topology of the system. As shown in Fig. 1(a), in topological phases I and III, there is a topological phase transition occurring along the k_z axis. For example, in phase III the phase boundary along the k_z direction corresponds to the emergence of two gapless points in quasiparticle excitations at $(\pi, \pi, \pm k_{III}^c)$, as shown in Fig. 6(a). It turns out that these two gapless points are Weyl nodes. For instance, the effective low-energy physics around the gapless point (π, π, k_{III}^c) can be captured by expanding $H_{p\text{-wave}}^{\prime\prime\pi}$ around that

point to the leading order and we obtain

$$H_{\text{eff}}^{\pi} = -\Delta(k_x a - \pi)\sigma_x + \Delta(k_y a - \pi)\sigma_y + \frac{\partial E_1^{\pi}}{\partial k_z} \Big|_{\mathbf{k}=(\pi/a, \pi/a, k_{III}^c/a_z)} (k_z a_z - k_{III}^c)\sigma_z.$$

It takes the form of a 2×2 Hamiltonian describing chiral Weyl fermions. The quasiparticle energy dispersion is linear around the Weyl point. To further visualize the topological nontrivial nature of the Weyl node, a vector field \mathbf{d} can be defined through the relation

$$\begin{aligned} \tilde{H}_{\text{eff}}^{\pi} &= \sigma_x H_{\text{eff}}^{\pi} \sigma_x \\ &= -\Delta(k_x a - \pi)\sigma_x - \Delta(k_y a - \pi)\sigma_y \\ &\quad - \frac{\partial E_1^{\pi}}{\partial k_z} \Big|_{\mathbf{k}=(\pi/a, \pi/a, k_{III}^c/a_z)} (k_z a_z - k_{III}^c)\sigma_z \\ &\equiv \mathbf{d} \cdot \boldsymbol{\sigma}. \end{aligned}$$

As shown in Figs. 6(b) and 6(c), the Weyl nodes are hedgehoglike topological defects of the vector field \mathbf{d} , which are the point source of Berry flux in momentum space, with a topological invariant $N_C = \mp 1$. Here N_C is defined by $N_C = \frac{1}{24\pi^2} \epsilon_{\mu\nu\gamma\chi} \text{tr} \int_{\tilde{\Sigma}} dS^{\chi} \tilde{G} \frac{\partial \tilde{G}^{-1}}{\partial k_{\mu}} \tilde{G} \frac{\partial \tilde{G}^{-1}}{\partial k_{\nu}} \tilde{G} \frac{\partial \tilde{G}^{-1}}{\partial k_{\gamma}}$, where \tilde{G}^{-1} is the inverse Green's function for the quasiparticle excitation, $\tilde{\Sigma}$ is a 3D surface around the isolated gapless points, and tr stands for the trace over the relevant particle-hole degrees of freedom. Quasiparticle excitations near the gapless points realize the long-sought low-temperature analogs of Weyl fermions originally proposed in particle physics. These Weyl nodes are separated from each other in momentum space. They cannot be hybridized, which makes them indestructible, as they can only disappear by mutual annihilation of pairs with opposite topological charges, which is distinct from the spectral-gap protection in insulating topological phases.

B. Dirac fermions

Furthermore, as shown in Fig. 1(a), when varying J , the system undergoes phase transitions between various topological phases. The phase boundaries correspond to the gap closing in quasiparticle excitations. Interestingly, we find that these gapless points develop low-temperature analogs of Dirac topological defect. For example, when considering the phase boundary between III and IV, since the gapless point satisfies the relation $\frac{\partial E_1^{\pi}}{\partial k_z} = 0$, we can obtain the effective Hamiltonian around the gapless point as

$$H_{\text{eff}}^{\prime\prime\pi} = -\Delta(k_x a - \pi)\sigma_x + \Delta(k_y a - \pi)\sigma_y.$$

It takes the form of the effective Hamiltonian describing Dirac fermions. To visualize this, the planar vector \mathbf{h} near the gapless point can be defined through the relation

$$\begin{aligned} \tilde{H}_{\text{eff}}^{\prime\prime\pi} &= \sigma_x H_{\text{eff}}^{\prime\prime\pi} \sigma_x = -\Delta(k_x a - \pi)\sigma_x - \Delta(k_y a - \pi)\sigma_y \\ &\equiv \mathbf{h} \cdot \boldsymbol{\sigma}. \end{aligned}$$

As shown in Fig. 7(b), the vector field \mathbf{h} forms a vortex structure in the momentum space. At the vortex core, the length of the vector vanishes, indicating the gap closing in quasiparticle excitations. Therefore, it forms a Dirac topological defect,

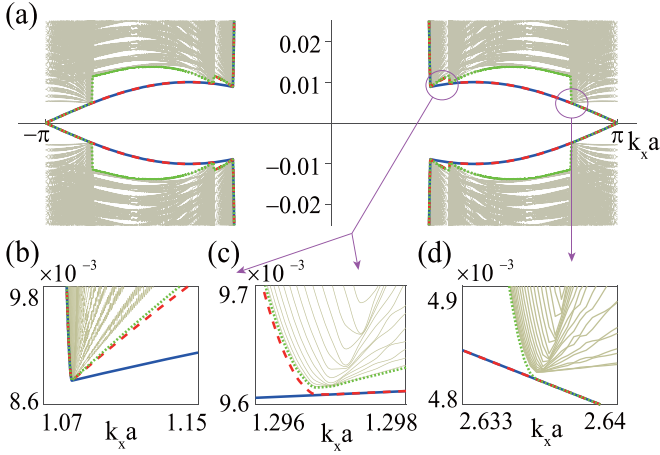


FIG. 9. Energy spectrum of the system with open (periodic) boundary conditions in the y (x) directions for a fixed k_z . (a) The blue, red, and green branches correspond to the three pairs of chiral edge modes in phase V, where $J = 1.1$, $n_0 = 0.77$, and $k_z a_z = 0$. (b)–(d) Close-ups of the part near the boundaries between the edge and bulk modes in (a). There are three pairs of zero-energy edge states, which turn out to be three Majorana fermions per edge. The other parameters are the same as in Fig. 1.

In summary, we have shown how to construct a toolbox for systematically engineering three kinds of emergent elementary fermions by utilizing one of the most desirable topological quantum states, i.e., $p + ip$ superfluids. A link between searching for fundamental particles and topological phenomena has been made. An experimentally plausible route to realize such an idea has been proposed in a spinless dipolar Fermi gas. The crucial ingredient of our proposal is the direction-dependent effective interaction between dipoles generated by a rotating external field, which has been realized in the experimental system of magnetic atoms [39]. This

approach requires neither spin-orbit coupling nor artificial gauge fields in general, automatically avoiding the challenge of their experimental realization in atomic Fermi gases. It has been shown that through simply tuning the designable dipolar interaction, the spontaneously formed density modulation provides a natural tool to manipulate the topological nature of the system and paves the way for transforming the fermion's nature of distinct elementary fermions. Both magnetic atoms and polar molecules in optical lattices are good candidates to provide a laboratory realization of our scheme. This systematic tool developed herein enables the controlled manipulation of various emergent elementary fermions, with applications ranging from fundamental physics to quantum computing.

ACKNOWLEDGMENTS

The authors thank Peter Zoller and W. Vincent Liu for helpful discussions. This work was supported by NSFC (Grants No. 12074305, No. 11774282, and No. 11950410491), the National Key Research and Development Program of China (Grant No. 2018YFA0307600), Cyrus Tang Foundation Young Scholar Program, and the Fundamental Research Funds for the Central Universities (S.L., M.A., and B.L.). H.L. was supported by NSFC Grant No. 11774284. F.L. was supported by NSFC Grant No. 11534008 and the National Key R&D Project (Grant No. 2016YFA0301404). We are also grateful to the HPC platform of Xi'an Jiaotong University, where our numerical calculations was performed.

APPENDIX A: EFFECTIVE HAMILTONIAN DESCRIBING THE CASE WITH $\mathbf{Q} = (0, 0, 2\pi/3a_z)$

Let us discuss the case of the period of z -directional CDW order being $3a_z$, characterized by $\mathbf{Q} = (0, 0, 2\pi/3a_z)$. The corresponding mean-field BdG Hamiltonian can be expressed as

$$H_{\text{BdG}}^{2\pi/3} = \begin{pmatrix} \xi_{\mathbf{k}-\mathbf{Q}} & \Delta(\mathbf{k}) & \delta & 0 & \delta & 0 \\ \Delta^*(\mathbf{k}) & -\xi_{-(\mathbf{k}-\mathbf{Q})} & 0 & -\delta & 0 & -\delta \\ \delta & 0 & \xi_{\mathbf{k}} & \Delta(\mathbf{k}) & \delta & 0 \\ 0 & -\delta & \Delta^*(\mathbf{k}) & -\xi_{-\mathbf{k}} & 0 & -\delta \\ \delta & 0 & \delta & 0 & \xi_{\mathbf{k}+\mathbf{Q}} & \Delta(\mathbf{k}) \\ 0 & -\delta & 0 & -\delta & \Delta^*(\mathbf{k}) & -\xi_{-(\mathbf{k}+\mathbf{Q})} \end{pmatrix}. \quad (\text{A1})$$

We then apply a unitary transformation to the BdG Hamiltonian above and obtain

$$\tilde{H}_{\text{BdG}}^{2\pi/3} = T_{2\pi/3}^\dagger H_{\text{BdG}}^{2\pi/3} T_{2\pi/3} = \begin{pmatrix} \xi_{\mathbf{k}-\mathbf{Q}} & \delta & \delta & \Delta(\mathbf{k}) & 0 & 0 \\ \delta & \xi_{\mathbf{k}} & \delta & 0 & \Delta(\mathbf{k}) & 0 \\ \delta & \delta & \xi_{\mathbf{k}+\mathbf{Q}} & 0 & 0 & \Delta(\mathbf{k}) \\ \Delta^*(\mathbf{k}) & 0 & 0 & -\xi_{-(\mathbf{k}-\mathbf{Q})} & -\delta & -\delta \\ 0 & \Delta^*(\mathbf{k}) & 0 & -\delta & -\xi_{-\mathbf{k}} & -\delta \\ 0 & 0 & \Delta^*(\mathbf{k}) & -\delta & -\delta & -\xi_{-(\mathbf{k}+\mathbf{Q})} \end{pmatrix},$$

with

$$T_{2\pi/3} = \begin{pmatrix} 1 & 0 & 0 & 0 & 0 & 0 \\ 0 & 0 & 0 & 1 & 0 & 0 \\ 0 & 1 & 0 & 0 & 0 & 0 \\ 0 & 0 & 0 & 0 & 1 & 0 \\ 0 & 0 & 1 & 0 & 0 & 0 \\ 0 & 0 & 0 & 0 & 0 & 1 \end{pmatrix}.$$

Then $\tilde{H}_{\text{BdG}}^{2\pi/3}$ can be further rewritten as

$$\tilde{H}_{\text{BdG}}^{2\pi/3} = \begin{pmatrix} H_{\text{CDW}}^{2\pi/3} & \Delta_k^{3\times 3} \\ \Delta_k^{*3\times 3} & -H_{\text{CDW}}^{2\pi/3} \end{pmatrix},$$

where

$$H_{\text{CDW}}^{2\pi/3} = \begin{pmatrix} \xi_{\mathbf{k}-\mathbf{Q}} & \delta & \delta \\ \delta & \xi_{\mathbf{k}} & \delta \\ \delta & \delta & \xi_{\mathbf{k}+\mathbf{Q}} \end{pmatrix}$$

and $\Delta_k^{3\times 3} = \Delta(\mathbf{k})I_{3\times 3}$, with $I_{3\times 3}$ the 3×3 unit matrix. After applying another unitary transformation to $\tilde{H}_{\text{BdG}}^{2\pi/3}$, we obtain

$$\mathcal{H}_{\text{BdG}}^{2\pi/3} = \Gamma_{2\pi/3}^\dagger \tilde{H}_{\text{BdG}}^{2\pi/3} \Gamma_{2\pi/3} = \begin{pmatrix} E_1^{2\pi/3} & 0 & 0 & \Delta(\mathbf{k}) & 0 & 0 \\ 0 & E_2^{2\pi/3} & 0 & 0 & \Delta(\mathbf{k}) & 0 \\ 0 & 0 & E_3^{2\pi/3} & 0 & 0 & \Delta(\mathbf{k}) \\ \Delta^*(\mathbf{k}) & 0 & 0 & -E_1^{2\pi/3} & 0 & 0 \\ 0 & \Delta^*(\mathbf{k}) & 0 & 0 & -E_2^{2\pi/3} & 0 \\ 0 & 0 & \Delta^*(\mathbf{k}) & 0 & 0 & -E_3^{2\pi/3} \end{pmatrix},$$

where the unitary transformation $\Gamma_{2\pi/3} = \begin{pmatrix} \Gamma_{2\pi/3\text{CDW}}^{2\pi/3} & 0_{3\times 3} \\ 0_{3\times 3} & \Gamma_{2\pi/3\text{CDW}}^{0_{3\times 3}} \end{pmatrix}$ can be defined through the relation

$$\Gamma_{2\pi/3\text{CDW}}^\dagger H_{\text{CDW}}^{2\pi/3} \Gamma_{2\pi/3\text{CDW}} = \begin{pmatrix} E_1^{2\pi/3}(\mathbf{k}) & 0 & 0 \\ 0 & E_2^{2\pi/3}(\mathbf{k}) & 0 \\ 0 & 0 & E_3^{2\pi/3}(\mathbf{k}) \end{pmatrix}.$$

Here $E_1^{2\pi/3}(\mathbf{k})$, $E_2^{2\pi/3}(\mathbf{k})$, and $E_3^{2\pi/3}(\mathbf{k})$ are the eigenspectra of $H_{\text{CDW}}^{2\pi/3}$ and, without loss of generality, we assume $E_1^{2\pi/3} \leq E_2^{2\pi/3} \leq E_3^{2\pi/3}$. Finally, we apply the unitary transformation $T_{2\pi/3}$ to $\mathcal{H}_{\text{BdG}}^{2\pi/3}$ and obtain

$$\begin{aligned} \mathcal{H}_{\text{BdG}}^{2\pi/3} &= T_{2\pi/3} \mathcal{H}_{\text{BdG}}^{2\pi/3} T_{2\pi/3}^\dagger = \begin{pmatrix} E_1^{2\pi/3} & \Delta(\mathbf{k}) & 0 & 0 & 0 & 0 \\ \Delta^*(\mathbf{k}) & -E_1^{2\pi/3} & 0 & 0 & 0 & 0 \\ 0 & 0 & E_2^{2\pi/3} & \Delta(\mathbf{k}) & 0 & 0 \\ 0 & 0 & \Delta^*(\mathbf{k}) & -E_2^{2\pi/3} & 0 & 0 \\ 0 & 0 & 0 & 0 & E_3^{2\pi/3} & \Delta(\mathbf{k}) \\ 0 & 0 & 0 & 0 & \Delta^*(\mathbf{k}) & -E_3^{2\pi/3} \end{pmatrix} \\ &\equiv \begin{pmatrix} H_{p\text{-wave}}^{2\pi/3} & 0_{2\times 2} & 0_{2\times 2} \\ 0_{2\times 2} & H_{p\text{-wave}}'^{2\pi/3} & 0_{2\times 2} \\ 0_{2\times 2} & 0_{2\times 2} & H_{p\text{-wave}}''^{2\pi/3} \end{pmatrix}. \end{aligned} \quad (\text{A2})$$

Therefore, the BdG Hamiltonian $H_{\text{BdG}}^{2\pi/3}$ can be decomposed into three effective Hamiltonians $H_{p\text{-wave}}^{2\pi/3}$, $H_{p\text{-wave}}'^{2\pi/3}$, and $H_{p\text{-wave}}''^{2\pi/3}$. Through analysis similar to that in the case of $\mathbf{Q} = (0, 0, \pi/a_z)$, we find that when $\mathbf{Q} = (0, 0, 2\pi/3a_z)$, the topological nature of the system can be tuned through simultaneously manipulating the topology of three effective Hamiltonians $H_{p\text{-wave}}^{2\pi/3}$, $H_{p\text{-wave}}'^{2\pi/3}$, and $H_{p\text{-wave}}''^{2\pi/3}$. For example, as shown in Fig. 10(a), through tuning the CDW order via varying the interaction strength J , the topological nature of the system can be engineered. Another four distinct topological phases can be achieved. Phases VI and VIII are characterized by uniform Chern numbers in the folded Brillouin zone along the k_z axis, i.e., $k_z a_z \in [-\frac{\pi}{3}, \frac{\pi}{3})$. The other two topological phases [V and VII in Fig. 10(a)] are characterized by the presence of a topological phase transition along the k_z axis, as shown in Fig. 10(b).

Applying the method similar to that in the case of $\mathbf{Q} = (0, 0, \pi/a_z)$, the low-energy effective Hamiltonian around

Weyl or Dirac nodes can also be obtained for $\mathbf{Q} = (0, 0, 2\pi/3a_z)$. For example, in phase VII we find that the effective low-energy physics around the gapless point $(\pi, \pi, k_{\text{VII}}^\xi)$ can be captured by

$$\begin{aligned} H_{\text{eff}}^{2\pi/3} &= -\Delta(k_x a - \pi)\sigma_x + \Delta(k_y a - \pi)\sigma_y \\ &+ \frac{\partial E_1^{2\pi/3}}{\partial k_z} \Big|_{\mathbf{k}=(\pi/a, \pi/a, k_{\text{VII}}^\xi/a_z)} (k_z a_z - k_{\text{VII}}^\xi)\sigma_z, \end{aligned}$$

which takes the form of a 2×2 Hamiltonian describing chiral Weyl fermions. While at the boundary between phases VII and VIII as shown in Fig. 10, since the gapless point satisfies the relation $\frac{\partial E_1^{2\pi/3}}{\partial k_z} = 0$, the effective Hamiltonian describing the low-energy physics around the gapless point can be captured by

$$H_{\text{eff}}^{2\pi/3} = -\Delta(k_x a - \pi)\sigma_x + \Delta(k_y a - \pi)\sigma_y,$$

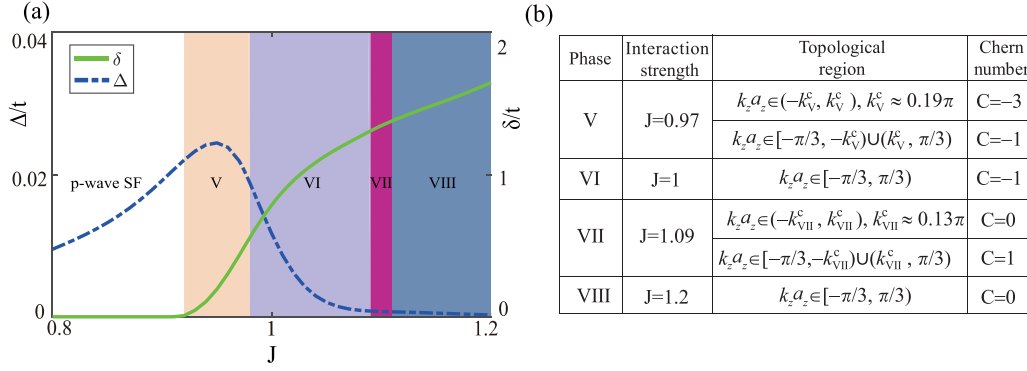


FIG. 10. (a) Zero-temperature phase diagram as a function of dipolar interaction strength at average filling $n_0 = 0.73$. The dashed and solid lines stand for the pairing and CDW order parameters, respectively. The spontaneously formed density modulation serves as a natural tool to manipulate the topological nature of the system, leading to distinct topological phases marked by various colors. (b) Table of examples showing the distinct topological nature of various phases in (a). The other parameters are the same as in Fig. 1.

which takes the form of the effective Hamiltonian describing Dirac fermions.

APPENDIX B: FINITE-TEMPERATURE PHASE TRANSITION

In our proposed anisotropic 3D lattice system, it turns out that the superfluid density in the z direction is much smaller than that on the xy plane, for instance, as shown in Fig. 11(c). Therefore, the superfluid transition temperature can be discussed within the framework of a highly anisotropic 3D XY model [51–55]. In such a case, the transition temperature is at most a few percent larger than T_{BKT} [52–54]. We can thus use the T_{BKT} to approximate the critical temperature, where T_{BKT} is determined by the relation [51–54] $k_B T_{\text{BKT}} = \frac{\pi}{2} \bar{J} (k_B T_{\text{BKT}})$ with $\bar{J} = \frac{J^x + J^y}{2}$, and $J^\alpha = n_{s,2D}^\alpha / 4m_\alpha$, where $m_\alpha = 1/2t_\alpha a_\alpha^2$ with $\alpha = x, y, z$. Here $n_{s,2D}^\alpha = n_s^\alpha a_z$ is the effective 2D areal

superfluid density [52] and $n_s^\alpha = \rho_s^\alpha N / N_L a^2 a_z$, where ρ_s^α can be obtained from the response function to the phase twist,

$$\rho_s^\alpha = \frac{2t_\alpha - \Sigma_\alpha}{2Nt_\alpha} \sum_{\mathbf{k}} [n_{\mathbf{k}} \cos(k_\alpha a_\alpha) - f_\alpha], \quad (\text{B1})$$

where

$$f_\alpha = -(2t_\alpha - \Sigma_\alpha) k_B T \sum_{\mathbf{k}'} \int_0^\beta \int_0^\beta d\tau d\tau' \sin(k_\alpha a_\alpha) \sin(k'_\alpha a_\alpha) \times [-\delta_{\mathbf{k}, -\mathbf{k}'} F(\mathbf{k}, \tau, \tau') F^\dagger(\mathbf{k}', \tau, \tau') - \delta_{\mathbf{k}, -\mathbf{k}' - \mathbf{Q}} \tilde{F}(\mathbf{k}, \tau, \tau') \tilde{F}^\dagger(\mathbf{k}', \tau, \tau') + \delta_{\mathbf{k}, \mathbf{k}'} G(\mathbf{k}, \tau, \tau') \times G^\dagger(\mathbf{k}', \tau, \tau') + \delta_{\mathbf{k}, \mathbf{k}' + \mathbf{Q}} \tilde{G}(\mathbf{k}, \tau, \tau') \tilde{G}^\dagger(\mathbf{k}', \tau, \tau')], \quad (\text{B2})$$

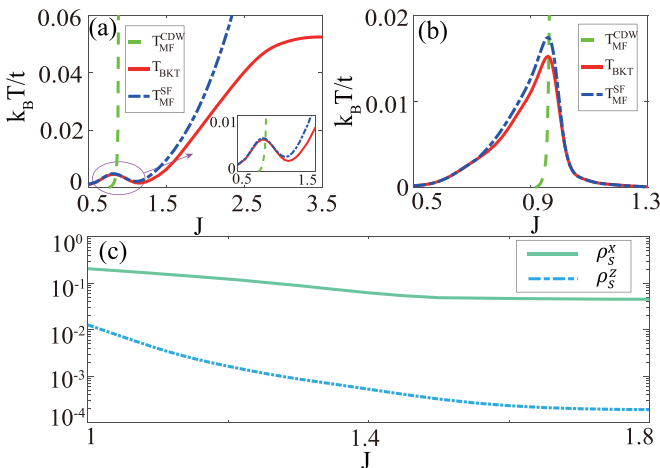


FIG. 11. Finite-temperature phase diagram as a function of dipolar interaction strength when the average filling (a) $n_0 = 0.6$ and (b) $n_0 = 0.73$. The blue and green lines show the mean-field transition temperature of the superfluid and CDW, respectively. The red line indicates the Berezinskii-Kosterlitz-Thouless transition temperature. (c) Superfluid density as a function of J . The other parameters are the same as in Fig. 1.

with G , F , \tilde{G} , and \tilde{F} the Green's functions defined as $G(\mathbf{k}, \tau, \tau') = -\langle T_\tau c_{\mathbf{k}}(\tau) c_{\mathbf{k}}^\dagger(\tau') \rangle$, $F(\mathbf{k}, \tau, \tau') = -\langle T_\tau c_{\mathbf{k}}(\tau) c_{-\mathbf{k}}(\tau') \rangle$, $\tilde{G}(\mathbf{k}, \tau, \tau') = -\langle T_\tau c_{\mathbf{k}}(\tau) c_{\mathbf{k}+\mathbf{Q}}^\dagger(\tau') \rangle$, and $\tilde{F}(\mathbf{k}, \tau, \tau') = -\langle T_\tau c_{\mathbf{k}}(\tau) c_{-\mathbf{k}-\mathbf{Q}}(\tau') \rangle$, respectively. In addition, N is the total number of particles.

Through the analysis above, we can obtain the finite-temperature phase diagram of our proposed system. For instance, when the average filling is $n_0 = 0.6$ [the case of $\mathbf{Q} = (0, 0, \pi/a_z)$], as shown in Fig. 11(a), T_{BKT} is approximately equal to the mean-field transition temperature of superfluids $T_{\text{MF}}^{\text{SF}}$ in the weak-interaction region. However, when increasing J , there is a discrepancy between T_{BKT} and $T_{\text{MF}}^{\text{SF}}$ as expected, because the mean-field analysis underestimates fluctuation effects. In a larger interacting coupling region, the CDW phase can survive higher temperatures, as indicated by the mean-field transition temperature $T_{\text{MF}}^{\text{CDW}}$. Therefore, below T_{BKT} , our proposed distinct topological phases, such as phases I–IV in Fig. 1, can be achieved at finite temperature. When the average filling is $n_0 = 0.73$ [the case of $\mathbf{Q} = (0, 0, 2\pi/3a_z)$], the finite-temperature phase diagram is obtained as shown in Fig. 11(b).

- [1] P. A. M. Dirac, *Proc. Roy. Soc. Lond. A* **117**, 610 (1928).
- [2] P. A. M. Dirac, *Proc. Roy. Soc. Lond. A* **126**, 360 (1930).
- [3] O. Klein, *Z. Phys.* **37**, 895 (1926).
- [4] H. Weyl, *Z. Phys.* **56**, 330 (1929).
- [5] E. Majorana, *Nuovo Cimento* **14**, 171 (1937).
- [6] A. Zee, *Quantum Field Theory in a Nutshell* (Princeton University Press, Princeton, 2010).
- [7] S. Weinberg, *The Quantum Theory of Fields* (Cambridge University Press, Cambridge, 2005), Vol. 1.
- [8] A. H. Castro Neto, F. Guinea, N. M. R. Peres, K. S. Novoselov, and A. K. Geim, *Rev. Mod. Phys.* **81**, 109 (2009).
- [9] M. O. Goerbig, *Rev. Mod. Phys.* **83**, 1193 (2011).
- [10] V. N. Kotov, B. Uchoa, V. M. Pereira, F. Guinea, and A. H. Castro Neto, *Rev. Mod. Phys.* **84**, 1067 (2012).
- [11] K. S. Novoselov, A. K. Geim, S. V. Morozov, D. Jiang, M. I. Katsnelson, I. V. Grigorieva, S. V. Dubonos, and A. A. Firsov, *Nature (London)* **438**, 197 (2005).
- [12] Y. Zhang, Y.-W. Tan, H. L. Stormer, and P. Kim, *Nature (London)* **438**, 201 (2005).
- [13] M. I. Katsnelson, K. S. Novoselov, and A. K. Geim, *Nat. Phys.* **2**, 620 (2006).
- [14] G. E. Volovik, *The Universe in a Helium Droplet* (Oxford University Press, Oxford, 2003).
- [15] M. Z. Hasan and C. L. Kane, *Rev. Mod. Phys.* **82**, 3045 (2010).
- [16] X.-L. Qi and S.-C. Zhang, *Rev. Mod. Phys.* **83**, 1057 (2011).
- [17] V. Galitski and I. Spielman, *Nature (London)* **494**, 49 (2013).
- [18] J. Dalibard, F. Gerbier, G. Juzeliūnas, and P. Öhberg, *Rev. Mod. Phys.* **83**, 1523 (2011).
- [19] Y.-J. Lin, K. Jimenez-Garcia, and I. B. Spielman, *Nature (London)* **471**, 83 (2011).
- [20] Z. Wu, L. Zhang, W. Sun, X.-T. Xu, B.-Z. Wang, S.-C. Ji, Y. Deng, S. Chen, X.-J. Liu, and J.-W. Pan, *Science* **354**, 83 (2016).
- [21] L. W. Cheuk, A. T. Sommer, Z. Hadzibabic, T. Yefsah, W. S. Bakr, and M. W. Zwierlein, *Phys. Rev. Lett.* **109**, 095302 (2012).
- [22] P. Wang, Z.-Q. Yu, Z. Fu, J. Miao, L. Huang, S. Chai, H. Zhai, and J. Zhang, *Phys. Rev. Lett.* **109**, 095301 (2012).
- [23] G. Jotzu, M. Messer, R. Desbuquois, M. Lebrat, T. Uehlinger, D. Greif, and T. Esslinger, *Nature (London)* **515**, 237 (2014).
- [24] L. Duca, T. Li, M. Reitter, I. Bloch, M. Schleier-Smith, and U. Schneider, *Science* **347**, 288 (2015).
- [25] M. Aidelsburger, M. Atala, M. Lohse, J. T. Barreiro, B. Paredes, and I. Bloch, *Phys. Rev. Lett.* **111**, 185301 (2013).
- [26] H. Miyake, G. A. Siviloglou, C. J. Kennedy, W. C. Burton, and W. Ketterle, *Phys. Rev. Lett.* **111**, 185302 (2013).
- [27] C. V. Parker, L.-C. Ha, and C. Chin, *Nat. Phys.* **9**, 769 (2013).
- [28] H. Zhai, *Int. J. Mod. Phys. B* **26**, 1230001 (2012).
- [29] S.-L. Zhang and Q. Zhou, *Phys. Rev. A* **90**, 051601(R) (2014).
- [30] W. Zheng and H. Zhai, *Phys. Rev. A* **89**, 061603(R) (2014).
- [31] S. K. Baur, M. H. Schleier-Smith, and N. R. Cooper, *Phys. Rev. A* **89**, 051605(R) (2014).
- [32] T. Müller, S. Fölling, A. Widera, and I. Bloch, *Phys. Rev. Lett.* **99**, 200405 (2007).
- [33] G. Wirth, M. Ölschläger, and A. Hemmerich, *Nat. Phys.* **7**, 147 (2011).
- [34] P. Soltan-Panahi, D.-S. Lühmann, J. Struck, P. Windpassinger, and K. Sengstock, *Nat. Phys.* **8**, 71 (2012).
- [35] T. Kock, M. Ölschläger, A. Ewerbeck, W.-M. Huang, L. Mathey, and A. Hemmerich, *Phys. Rev. Lett.* **114**, 115301 (2015).
- [36] M. C. Rechtsman, J. M. Zeuner, Y. Plotnik, Y. Lumer, D. Podolsky, F. Dreisow, S. Nolte, M. Segev, and A. Szameit, *Nature (London)* **496**, 196 (2013).
- [37] A. B. Khanikaev, S. Hossein Mousavi, W.-K. Tse, M. Kargarian, A. H. MacDonald, and G. Shvets, *Nat. Mater.* **12**, 233 (2013).
- [38] M. A. Baranov, M. Dalmonte, G. Pupillo, and P. Zoller, *Chem. Rev.* **112**, 5012 (2012).
- [39] Y. Tang, W. Kao, K.-Y. Li, and B. L. Lev, *Phys. Rev. Lett.* **120**, 230401 (2018).
- [40] M. Lu, N. Q. Burdick, and B. L. Lev, *Phys. Rev. Lett.* **108**, 215301 (2012).
- [41] K. Baumann, N. Q. Burdick, M. Lu, and B. L. Lev, *Phys. Rev. A* **89**, 020701(R) (2014).
- [42] K. Aikawa, A. Frisch, M. Mark, S. Baier, R. Grimm, and F. Ferlaino, *Phys. Rev. Lett.* **112**, 010404 (2014).
- [43] K. Aikawa, S. Baier, A. Frisch, M. Mark, C. Ravensbergen, and F. Ferlaino, *Science* **345**, 1484 (2014).
- [44] D. Ceperley, G. V. Chester, and M. H. Kalos, *Phys. Rev. B* **16**, 3081 (1977).
- [45] C. Gros, *Ann. Phys. (NY)* **189**, 53 (1989).
- [46] E. Neuscamman, C. J. Umrigar, and G. K.-L. Chan, *Phys. Rev. B* **85**, 045103 (2012).
- [47] R. Jastrow, *Phys. Rev.* **98**, 1479 (1955).
- [48] S. Sorella, *Phys. Rev. B* **64**, 024512 (2001).
- [49] B. A. Bernevig and T. L. Hughes, *Topological Insulators and Topological Superconductors* (Princeton University Press, Princeton, 2013).
- [50] A. Frisch, M. Mark, K. Aikawa, F. Ferlaino, J. L. Bohn, C. Makrides, A. Petrov, and S. Kotochigova, *Nature (London)* **507**, 475 (2014).
- [51] V. Cataudella and P. Minnhagen, *Physica C* **166**, 442 (1990).
- [52] B. Chattopadhyay and S. R. Shenoy, *Phys. Rev. Lett.* **72**, 400 (1994).
- [53] M. Friesen, *Phys. Rev. B* **51**, 632 (1995).
- [54] S. W. Pierson, *Phys. Rev. B* **51**, 6663 (1995).
- [55] P. Minnhagen and P. Olsson, *Phys. Rev. B* **44**, 4503 (1991).